

# Constraining inputs to realistic kilonova simulations through comparison to observed $r$ -process abundances

M. Ristic,<sup>1</sup> E. M. Holmbeck,<sup>2,3,4</sup> R. Wollaeger,<sup>5,6</sup> O. Korobkin,<sup>5,6</sup> E. Champion,<sup>7</sup> R. O’Shaughnessy,<sup>1</sup> C. L. Fryer,<sup>5,6,8,9</sup> C. J. Fontes,<sup>5,10</sup> M. R. Mumpower,<sup>4,5,11</sup> and T. M. Sprouse<sup>4,5,11</sup>

<sup>1</sup>*Center for Computational Relativity and Gravitation, Rochester Institute of Technology, Rochester, New York 14623, USA*

<sup>2</sup>*Observatories of the Carnegie Institution for Science, Pasadena, CA 91101, USA*

<sup>3</sup>*Hubble Fellow*

<sup>4</sup>*Joint Institute for Nuclear Astrophysics—Center for the Evolution of the Elements, USA*

<sup>5</sup>*Center for Theoretical Astrophysics, Los Alamos National Laboratory, Los Alamos, NM, 87545, USA*

<sup>6</sup>*Computer, Computational, and Statistical Sciences Division, Los Alamos National Laboratory, Los Alamos, NM, 87545, USA*

<sup>7</sup>*Department of Physics and Astronomy, University of Rochester, Rochester, NY 14627, USA*

<sup>8</sup>*The University of Arizona, Tucson, AZ 85721, USA*

<sup>9</sup>*Department of Physics and Astronomy, The University of New Mexico, Albuquerque, NM 87131, USA*

<sup>10</sup>*Computational Physics Division, Los Alamos National Laboratory, Los Alamos, NM, 87545, USA*

<sup>11</sup>*Theoretical Division, Los Alamos National Laboratory, Los Alamos, NM 87545, USA*

(Dated: June 7, 2022)

Kilonovae, one source of electromagnetic emission associated with neutron star mergers, are powered by the decay of radioactive isotopes in the neutron-rich merger ejecta. Models for kilonova emission consistent with available modeling and the electromagnetic counterpart to GW170817 also predict characteristic abundance patterns, determined by the relative balance of different types of material in the outflow. Assuming the observed source is prototypical, this inferred abundance pattern in turn must match  $r$ -process abundances deduced by other means, such as what is observed in the solar system. We report on analysis comparing the input mass-weighted elemental compositions adopted in our radiative transfer simulations to the mass fractions of elements in the Sun. We characterise the extent to which our parameter inference results depend on our assumed composition for the dynamical and wind ejecta and examine how the new results compare to previous work. We find that a mass ratio of  $M_w/M_d = 2.81$  reproduces the observed AT2017gfo kilonova light curves while also producing the abundance of neutron-capture elements in the solar system.

## I. INTRODUCTION

For nearly half a century, neutron star (NS) binaries have been known to exist in nature, stemming from the first detection of a binary pulsar system [1]. Shortly thereafter, the general relativistic prediction of gravitational radiation from a compact object binary was measured in the same system, implying the possibility of neutron star binary coalescence [2]. Recently, neutron star mergers were confirmed as astrophysical sources of both gravitational wave (GW) and electromagnetic (EM) emission with the detection of the binary neutron star merger GW170817 [3].

Around the same time as the first pulsar binary detection, compact object mergers involving neutron stars, either binary neutron star (BNS) or black-hole-neutron-star (BHNS), were predicted to be candidates for rapid neutron capture ( $r$ -process) nucleosynthesis [4]. The nuclei synthesized in the post-merger ejecta were thought to be heavy ( $A > 140$ ), radioactive isotopes which have short lifetimes due to their instability [5]. As these nuclei decayed, they would release energy into the surrounding matter which would be emitted as thermal radiation once the ejecta became optically thin [6]. This thermal emission is now commonly referred to as a kilonova and serves as the bridge between the  $r$ -process elements produced by neutron star mergers and their resultant electromagnetic emission [7–9].

Previous studies have highlighted the importance of nuclear physics inputs on  $r$ -process nucleosynthesis and the resultant effect on observed kilonova emission [10, 11]. In this work, we build on quantifying the effects of nuclear physics inputs by utilizing detailed line-binned opacity calculations to examine how variations in the nuclear physics inputs for both the dynamical and wind ejecta affect  $r$ -process element production and kilonova observables.

The material ejected from BNS mergers like GW170817 therefore produces two currently observationally accessible signatures: electromagnetic kilonova emission from individual transients and relic  $r$ -process abundances from stars (e.g., metal-poor stars or the Sun). This project combines nucleosynthetic yield constraints assuming  $r$ -process contribution exclusively from NS mergers and EM constraints assuming all NS mergers look like GW170817. We investigate the effects of comparing elemental abundances from kilonova simulations to the solar  $r$ -process abundance under the assumption that second and third  $r$ -process peaks follow universal behavior. We use this comparison to create a parameter estimation prior driven by explicit consideration of  $r$ -process elemental abundances in kilonova ejecta to gauge the effects on recovered ejecta properties. As kilonova models improve in complexity and more observations become available for parameter estimation purposes, we can utilize more representative simulation abundances to

hone this prior in future studies.

In this work, we will assess the extent to which our assumptions about the ejected material are simultaneously consistent with both types of aforementioned observations. Specifically, we will examine whether the abundances produced by our merger simulations realistically match the  $r$ -process abundances observed in the Sun. In Section II A, we discuss the atomic and nuclear physics codes used to calculate the line-binned opacities and dynamical ejecta compositions, respectively, considered in this work. In Section II B, we described our method of comparing mass-weighted  $r$ -process abundances from our simulations with the solar abundance pattern. Section II C describes our parameter estimation framework and the effects of the  $r$ -process prior introduced in this work. In Section III we discuss whether the inclusion of the  $r$ -process prior makes a substantial difference in the parameter estimation process compared to prior work.

## II. METHODS

### A. Simulation Setup

Our methodology follows from [12, 13] and references therein. In brief, we use the detailed, time-dependent radioactive isotope composition results from the nucleosynthesis simulations with the WinNet code [14] to determine nuclear heating rates via contributions of individual radiation species (such as  $\alpha$ -,  $\beta$ -,  $\gamma$ -radiation, and fission products) for each isotope. These contributions are also weighted by thermalization efficiencies first presented in [15] (see [12] for a detailed description of the adopted nuclear heating). These heating rates and composition effects, in conjunction with tabulated binned opacities generated with the Los Alamos suite of atomic physics codes [16, 17], yield the kilonova light curves used in our parameter estimation process (see Section II C). Our tabulated binned opacities are not calculated for all elements; therefore, we produce opacities for representative proxy elements by combining pure-element opacities of nuclei with similar atomic properties [17].

The compositions presented in this work were generated using two nuclear network codes: WinNet and PRISM. The dynamical and wind ejecta compositions considered here and in previous work (i.e. [12, 13]) were generated using WinNet. The varied dynamical ejecta compositions new to this work were generated using PRISM. PRISM is a single-zone nuclear reaction network code that evolves an initial seed abundance of nuclei along a time-temperature-density thermodynamic trajectory, while allowing full flexibility with the input nuclear data [18]. In this work, we use state-of-the-art nuclear reaction and decay rates that are calculated to be self-consistent with the nuclear mass model. Following from the thermodynamic trajectories of dynamical ejecta from neutron star merger simulations presented in [7], all of our PRISM runs begin in nuclear statistical equilibrium at a temperature

of 10 GK in the thermodynamic trajectory.

Our kilonova light curve model assumptions and interpolation follow directly from [13]. In summary, our radioactive heating considerations are the same as for the “dynamical,” “wind1,” and “wind2” models in [12]. Each of our two ejecta components, dynamical and wind, is described by a fixed elemental composition and morphology. The elemental compositions are varied in this work, but the morphologies are fixed to torus-shaped and peanut-shaped for the dynamical and wind ejecta, respectively (see [19] for a detailed discussion on morphologies).

We interpolate using Gaussian process (GP) regression with a squared-exponential kernel and a white noise (diagonal) kernel. Unless otherwise noted, we quantify the performance of our interpolation with the RMS difference between our prediction and the true value. Because of the substantial dynamic range of our many outputs, we interpolate in AB magnitudes using the LSST *grizy* and 2MASS *JHK* bands as our reference wavelengths. Our raw light curve models are calculated assuming a fiducial source distance of 10 parsecs.

### B. Ejecta Prior Implied by $r$ -process Observations

In our SuperNu simulations, we adopt a two-component compositional model and vary the mass ratio of the two components: the dynamical ( $M_d$ ) and wind ( $M_w$ ) ejecta. Each component has a fixed isotopic abundance, computed via nucleosynthesis network [14]. For every isotope, the combined mass fraction is simply the mass-weighted sum of its mass fractions in the constitutive components. Due to the fixed nature of the compositions, we weight each component’s composition by the mass of the respective ejecta component, dynamical  $M_d$  or wind  $M_w$ , to introduce composition variation as a function of component mass. We varied our dynamical and wind component masses over a grid between  $-3 \leq \log(M_{d,w}/M_\odot) \leq -1$ , encompassing the most realistic ejecta masses predicted by numerical relativity simulations of neutron star mergers [20–25].

As discussed in Section I, we want to compare the combined mass fractions  $X_{sim} = M_w X_w + M_d X_d$  to the seemingly universal pattern of elements between the 2nd and 3rd  $r$ -process peaks (the “main”  $r$ -process, [9]). This “ $r$ -process universality” has been noted for iron-poor (or “metal-poor”) stars that show enhancements in the main  $r$ -process elements relative to their iron content. However, abundance patterns of metal-poor stars are necessarily elemental since the abundances are derived from atomic transitions in stellar spectra. Except for a handful of elements, the detailed *isotopic* distributions of  $r$ -process elements in metal-poor stars is observationally unknown. As a proxy for a representative example of the universal  $r$ -process, we use the well-studied solar isotopic abundance pattern, relying on previously-published projections of the high- $A$  elements into different neutron-capture process contributions. Specifically, the  $r$ -process

fractions presented in [26] are used in conjunction with the total abundances from [27] to isolate the contribution to the solar abundances by the  $r$ -process.

We rescale the solar mass fractions of actinides  $X_{\odot,Ac}$  to what they would have been at 1 day to better match the kilonova-timescale mass fractions used in our simulations. The rescaling is achieved by setting the “1-day” solar actinide mass fractions to values that would decay to present day values after 4.5 Gyr. The rescaled solar mass fractions are also mapped into a subset of representative elements with the computed tabulated binned opacities discussed in Section II A. Hereafter, any mention of the solar mass-fraction pattern  $X_{\odot}$  refers to the “1-day” rescaled and mapped mass fractions using data from [26] and [27].

To get  $X_{\odot}$  and  $X_{sim}$  on the same relative scale, we introduce an offset  $C_{scale}$  that shifts  $X_{\odot}$  down to comparable values for  $X_{sim}$  by matching the two mass-fraction values at some element  $Z$ . To minimize how the choice of  $C_{scale}$  affects our results, we integrate over all possible values of  $C_{scale}$  introduced by scaling  $X_{\odot}$  and  $X_{sim}$  to matching values at different elements  $Z$ . After integrating over  $C_{scale}$ , we are left with a single required choice of a new  $C$  value that sets the scale at some element  $Z_{choice}$  such that  $C = X_{\odot,Z_{choice}} - X_{sim,Z_{choice}}$ . We chose  $Z_{choice} = 46$  as it is one of the elements present in all the dynamical, wind, and solar mass fractions. We note that shifting  $X_{\odot}$  to be on the same relative scale as  $X_{sim}$  and choosing a specific value of  $C$  at some  $Z_{choice}$  are both done solely for the purpose of calculating well-behaved likelihoods.

Figure 1 shows the  $[X/Fe]$  abundances of six metal-poor stars. The “[X/Fe]” notation means that each elemental ratio  $\log \epsilon(X/Fe)$  is compared to the same elemental ratio in the solar abundance pattern.<sup>1</sup> Stars with  $[X/Fe] > 0$  are considered “enhanced” in that element relative to the solar system abundance. For many metal-poor stars, elements with  $Z \geq 37$  have an enhanced abundance compared to iron. With the assumption that iron was created during supernova nucleosynthesis, we assume all elements that are enhanced compared to iron to have been introduced post-supernova. For this work, we assume that elements with  $Z \geq 37$  originate from neutron star mergers. The trends of elements with  $Z < 37$  are less clear; they are not uniformly enhanced in stars that are enhanced with the  $Z \geq 37$  elements, likely pointing to multiple (non-merger) origins for these elements. Therefore, we only consider elements from  $Z_{min} = 37$  up to and including  $Z_{max} = 102$  when we compute the residual  $r(M_d, M_w)$  for all available elements in the solar abundance pattern  $Z \in Z_{\odot}$  given a simulation with

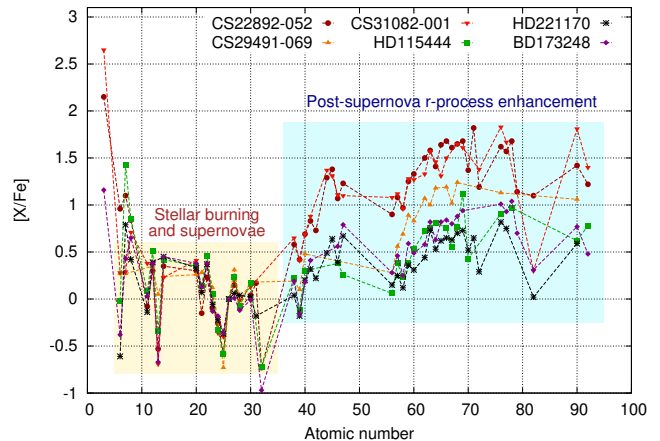


FIG. 1. Elemental mass fraction ratios relative to iron of a sample of  $r$ -process enriched metal-poor stars.  $[X/Fe] > 0$  implies enhanced abundance of element  $X$  compared to the solar system with respect to iron. We assume all elements that are significantly enhanced compared to iron to have been introduced post-supernova. The region of enhanced elements ( $Z \geq 37$ , highlighted in blue) is the focus of our comparison to solar composition. The iron-peak elements and supernova  $r$ -process are not strongly enhanced compared to Solar (highlighted in yellow). Stellar elemental abundances obtained from JINAbase [28] with the respective stars reported in references [29–34].

component masses  $M_d, M_w$ :

$$r(M_d, M_w) = \sum_{Z=Z_{min}}^{Z_{max}} \frac{(\log X_{\odot,Z} - \log C - \log X_{sim,Z})^2}{2\sigma^2} - \frac{N}{2\sigma^2} \frac{(\log \bar{X}_{sim} - \log \bar{X}_{\odot})^2}{1 + \sigma^2/(N\sigma_C^2)} \quad (1)$$

where  $r(M_d, M_w)$  is the residual for the given dynamical and wind mass pair used to calculate  $X_{sim} = M_w X_w + M_d X_d$ ,  $Z$  is the element’s atomic number,  $\log X_{\odot,Z}$  is the decimal logarithm of the solar mass fraction of element  $Z$ ,  $\log C$  is the decimal logarithm of the offset matching  $X_{\odot}$  to  $X_{sim}$  at  $Z = 46$ ,  $\log X_{sim,Z}$  is the decimal logarithm of the simulation mass fraction of element  $Z$  in both components (if present),  $\sigma$  is the uncertainty on  $\log X_{sim}$ ,  $\sigma_C$  is the uncertainty introduced by integrating out  $C_{scale}$ ,  $\bar{X}_{\odot}$  is the average solar mass fraction across all elements,  $\bar{X}_{sim}$  is the average simulation mass fraction across all elements, and  $N$  is the total number of elements considered.

Across a grid of  $M_d$  and  $M_w$ , we compute the likelihood by minimizing the residual from Equation 1. The top panel of Figure 2 shows the two-dimensional distribution of mass-pair likelihoods as a function of the dynamical and wind ejecta mass pairs from our grid, using wind and dynamical morphologies and compositions from [13] (see Section III for details). The bottom panel of Figure

<sup>1</sup> Definition:  $[X/Fe] := \log(Y_X/Y_{Fe}) - \log(Y_X/Y_{Fe})_{\odot}$ , where  $Y_X$  is the *abundance* (mole fraction) of the element  $X$ .

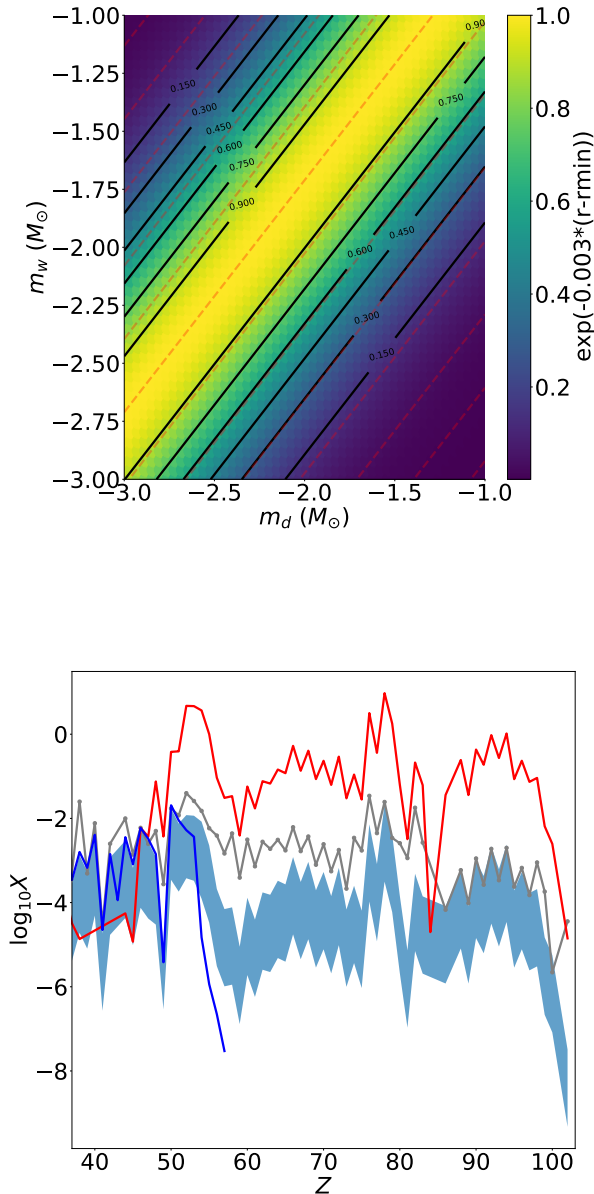


FIG. 2. *Top*: 2D distribution of likelihoods for 50 masses spread equally log-spaced between  $-3 \leq \log M_{\odot} \leq -1$  for dynamical and wind masses. The dynamical and wind compositions considered in creating this figure match those in [13] and are represented by the (\*) in Table I. *Bottom*: Composition of individual components in terms of mass fractions  $X_Z$  compared to the mass fractions of the solar  $r$ -process residuals. The red and blue lines are the initial unweighted dynamical and wind ejecta mass fractions, respectively, scaled to match the solar mass fraction at  $Z = 46$ . The gray line is the solar mass fraction and the blue shaded region is the 90% confidence interval for all the mass-weighted mass fractions  $\log X_{sim}$ . The dynamical ejecta mass fraction only exceeds  $\log X = 1$  due to the scale matching at  $Z = 46$ .

2 shows the individual component abundance patterns whose combination with  $M_d$  and  $M_w$  were compared to the solar pattern when computing the residual.

### C. Parameter Inference

As in many previous applications of Bayesian inference to infer parameters of kilonovae [35–42], we seek to compare the observed magnitudes  $x_i$  at evaluation points  $i$  (denoting a combination of band and time) to a continuous model that makes predictions  $m(i|\theta)$  [henceforth denoted by  $m_i(\theta)$  for brevity] which depend on some model parameters  $\theta$ . Bayes theorem expresses the posterior probability  $p(\theta)$  in terms of a prior probability  $p_{\text{prior}}(\theta)$  for the model parameters  $\theta$  and a likelihood  $\mathcal{L}(\theta)$  of all observations, given the model parameters, as

$$p(\theta) = \frac{\mathcal{L}(\theta)p_{\text{prior}}(\theta)}{\int d\theta \mathcal{L}(\theta)p_{\text{prior}}(\theta)}. \quad (2)$$

Unless otherwise noted, for simplicity we assume that the source sky location, distance, and merger time are known. We adopt a uniform prior on the ejecta velocity  $v/c \in [0.05, 0.3]$  and the two-dimensional prior discussed in Section II B on the ejecta masses  $m/M_{\odot} \in [0.001, 0.1]$ .

## III. RESULTS

For our two-component models, assuming a single source like GW170817 dominates the observed solar  $r$ -process abundances, the inferred abundances from such mergers only depend on the mass ratio  $M_w/M_d$ . In other words, since in our study we emphasize only the relative and not absolute  $r$ -process abundances, motivated by considerable uncertainty in the BNS merger rate, we therefore only use and constrain the abundance *ratios*. The relative abundances from a single channel only depend on the relative proportions of this channel; for our two-component model, thus just on  $M_w/M_d$ . Thus for each set of initial assumptions—the composition of the dynamical ejecta ( $Y_e$ ), the presumed nuclear mass and fission model, and other details—our comparison with solar abundances necessarily constrains  $M_w/M_d$  narrowly around a preferred value, unique to that model. We note that the abundances we are considering are effectively frozen out for the processes we’re interested in at times later than  $\mathcal{O}(1-2)$  seconds.

Table I provides a list of models and their preferred  $M_w/M_d$ , in the sense that they minimize the residual mismatch with the solar abundances as calculated in Equation 1. With a few exceptions, most models prefer  $M_w/M_d$  slightly above but close to unity. In other words, most of our abundance comparisons suggest somewhat more wind than dynamical ejecta would be required for GW170817-like mergers to reproduce the solar  $r$ -process abundances. These results are consistent with those

Trajectory	Mass Model	Fission Model	$Y_e$	Mass Ratio ( $M_w/M_d$ )	Min. Residual
Wind 2	FRDM2012	FRLDM	0.035	2.81	355
Wind 2	FRDM2012	50/50	0.180	1.60	684
Wind 2 (*)	FRDM2012	Panov+ (2010)	0.035	1.76	784
Wind 2	HFB24	FRLDM	0.180	1.60	832
Wind 2	HFB24	FRLDM	0.035	4.09	865
Wind 1	FRDM2012	FRLDM	0.035	0.32	927
Wind 1	HFB24	FRLDM	0.035	0.10	1436
Wind 1	FRDM2012	50/50	0.180	1.21	1474
Wind 1	FRDM2012	Panov+ (2010)	0.035	13.90	2079
Wind 1	HFB24	FRLDM	0.180	9.54	2144

TABLE I. Wind-to-dynamical mass ratios and minimum residuals for each dynamical composition considered. Mass ratios were determined by calculating the mean mass ratio of the bottom 2nd percentile of all residuals so as to eliminate outliers. The residuals were calculated as in Equation 1 and the minimum residual was identified as the smallest residual across all the mass pairs considered for a given composition. The two “Wind 1” and “Wind 2” trajectories are described in [13]. The two nuclear mass models considered are FRDM2012 and HFB24 [43, 44]. The two nuclear fission models considered in our study are FRLDM [43] and “50/50,” a simple symmetric assumption that fission yields split into two identical nuclei. The fission rates for the simulations performed in previous work, labeled Panov+ (2010), are taken from [45]. The (\*) indicates the compositions used in creating the surrogate light curves used during parameter estimation (see Section III).

found from other contemporary modeling [37, 41, 46, 47] as well as numerical relativity results [20, 25, 48–50]. The top panel of Figure 2 shows the preferred  $M_w/M_d$  ratio for the compositions, displayed in the bottom panel, used in [13], indicated by the (\*) in Table I. Figure 3 conveys the same information for the composition with the lowest residual compared to solar in our study. There is a clear increase in the ratio of wind to dynamical ejecta mass as can be seen in the mass ratio column of Table I as well as the recovered ejecta mass posteriors in Figure 5.

For each set of initial assumptions, the inferred constraint on  $M_w/M_d$  therefore also strongly constrains the ingredients powering the associated kilonova. For example, Figure 4 shows the results of inferring the parameters of GW170817, using *only* our prior constraints on  $M_w/M_d$  from the top panel of Figure 3 (and weak constraints on the binary orientation relative to our line of sight). Figure 5 shows how these constraints propagate into joint electromagnetic inference. The solid black contours show inferences derived without using constraints on  $M_w/M_d$ ; the red contours show inferences supplemented with this insight, for a specific set of initial assumptions. Even allowing for extremely conservative systematic uncertainties on these inputs (e.g., assuming  $M_w/M_d$ ’s optimal value is well-localized between 10 and 0.1) these prior abundance constraints should still provide useful insight into kilonova ejecta modeling.

Each set of our input assumptions about ejecta composition and physics makes a prediction about  $r$ -process abundances. As shown by the last column in Table I, some of our input assumptions fit better than others. Given substantial systematic uncertainties associated in the many assumptions in our study, we approach these

nominal residuals with considerable cautions. However, the minimum residuals presented in Table I suggest that the “wind2” model is a notably better fit to the solar mass-fraction pattern. The sharply-divided separation of the two wind models’ lowest residuals implies that the “wind1” model is less indicative of  $r$ -process nucleosynthesis from neutron star mergers. More importantly, the separation between the models also implies that new models for the wind ejecta composition need to be considered in comparison to the “wind2” model. The results of Table I indicate the need for further studies involving updated wind ejecta composition modeling informed by GRMHD disk simulations [24].

Our results can be improved by incorporating the observed higher variability of the lighter  $r$ -process abundances between the first and the second peak, compared to the universal pattern between the second and third  $r$ -process peaks. The lighter  $r$ -process as observed in metal-poor stars, exhibits variation on the order of 1 dex, while the “strong”  $r$ -process pattern varies by only about 0.3 dex [9]. An investigation with more accurate numbers based on careful statistical analysis of observations will be the subject of future studies [52].

Another caveat that presents limitations to our results is that we only incorporated very specific “wind1” and “wind2” compositions. There can be a broad variety of compositions permitted for electron fractions  $Y_e > 0.20$  due to varying hydrodynamic conditions. An extensive study of these compositions, along with the tests of how much they can be considered “representative” of their respective components, is beyond the scope of this work.

Finally, we note that we cannot ignore the bias introduced by the dynamical ejecta composition of the sur-

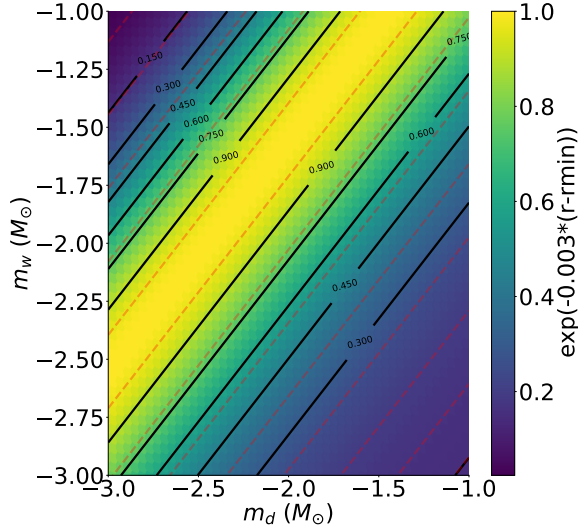


FIG. 3. *Top*: Same 2D distribution as described in Figure 2 except with the compositions which yielded the lowest residual in comparison to the solar abundance pattern (top row of Table I). *Bottom*: Composition of individual components in terms of mass fractions  $X_Z$  compared to the mass fractions of the solar  $r$ -process residuals. The line colors represent the same quantities as in Figure 2. The minimum residual was identified as the smallest residual across all the mass pairs considered for a given composition.

rogate kilonova light curves presented in [13]. While the constraints imposed by the  $r$ -process abundance prior indeed shift the recovered parameters as in Figure 5, there still remains some contribution to the parameter estima-

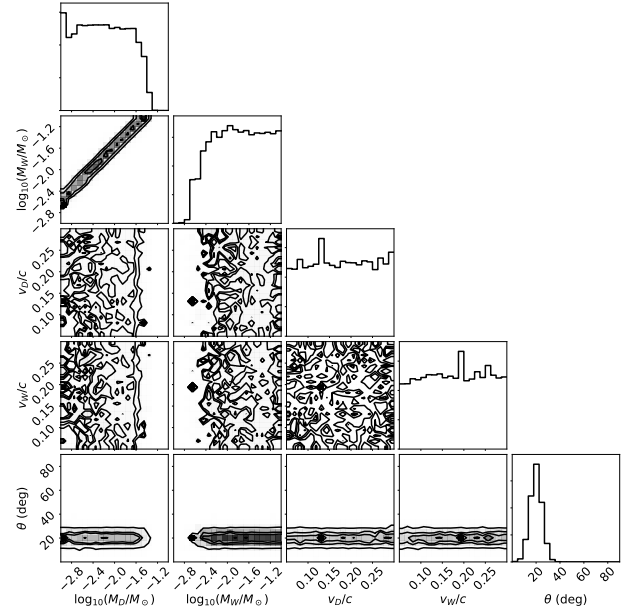


FIG. 4. Posterior distributions created using only the 2-D  $r$ -process prior presented in Figure 3 with no EM information provided during sampling besides constraints on the opening angle (see [51] and references therein). Note the recovery of the yellow band of lowest-residual mass pairs from Figure 3 in the  $M_W$  vs.  $M_D$  panel as well as the flat velocity posteriors stemming from the lack of velocity constraints introduced by our mass-focused prior. Residual small-scale substructure in the one- and two-dimensional marginal distributions reflects sample size artifacts. See Figure 5 for comparison.

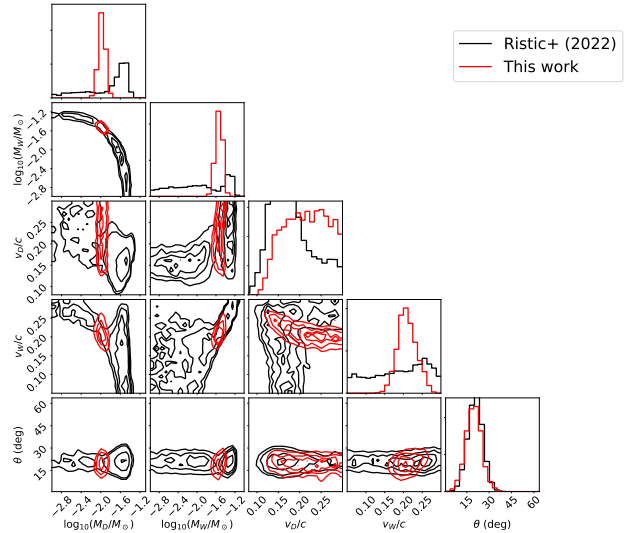


FIG. 5. Posterior distributions for samples generated when using the *grizyJHKS* bands considered in [13] (black) and samples generated using the same bands along with the  $r$ -process prior from Figure 3 (red). There is a clear shift in the recovered parameters with all but the dynamical velocity becoming more constrained.

tion stemming from the surrogate models having been trained on a different dynamical ejecta composition. In other words, our surrogate light curves were trained using the starred ejecta compositions in Table I. Although the primary contribution to the parameter inference in this work comes from the prior discussed in Section II B, there will be some bias from the surrogates’ original compositions.

#### IV. CONCLUSION

We have presented an approach for incorporating nuclear physics-based composition effects as a prior for our kilonova parameter inference framework. With the assumption that the general population of neutron star mergers will follow consistent  $r$ -process nucleosynthesis patterns, our approach allows for identification of best-fitting kilonova component compositions compared to the solar abundance. We considered a range of models with varying nuclear physics input, and, given the assumptions discussed above, the best-fitting model appears to be the one with FRDM2012 nuclear mass, FRLDM fission,  $Y_e = 0.035$  (extreme neutron richness in dynamical ejecta), “wind 2” moderately neutron-rich composition, and a high mass ratio:  $M_w/M_d = 2.81$ . However, our conclusions should be taken with care, since the number of input compositions considered were quite limited.

Our method as stated assumes that a narrow distribution of mergers in total mass  $M_{tot} = M_1 + M_2$  dominates nucleosynthesis yields. While self-evidently consistent with the BNS population inferred from the merging Galactic NS binaries, this assumption could even still hold for a wider BNS population as suggested by GW observations, if ejecta are (as expected) suppressed for

the most massive mergers with large  $M_{tot}$ .

In this work, we have considered fiducial initial conditions for the outflow, including composition, without allowing for correlations induced by the fact that both the composition and outflows are initialized by BNS mergers. In future work, we will explore self-consistent initialization from merger properties, in particular exploring the effects of binary mass ratio and NS remnant lifetime, which should have significant impact on the ejecta amount and composition [53–55].

#### V. ACKNOWLEDGMENTS

ROS, MR and EMH acknowledge support from NSF AST 1909534. EMH acknowledges additional support for this work by NASA through the NASA Hubble Fellowship grant HST-HF2-51481.001, awarded by the Space Telescope Science Institute, which is operated by the Association of Universities for Research in Astronomy, Inc., for NASA, under contract NAS5-26555. CLF, CJF, OK, RW, and EAC were supported by the US Department of Energy through the Los Alamos National Laboratory. Los Alamos National Laboratory is operated by Triad National Security, LLC, for the National Nuclear Security Administration of U.S. Department of Energy (Contract No. 89233218CNA000001). Research presented in this article was supported by the Laboratory Directed Research and Development program of Los Alamos National Laboratory under project number 20190021DR. This research used resources provided by the Los Alamos National Laboratory Institutional Computing Program, which is supported by the U.S. Department of Energy National Nuclear Security Administration under Contract No. 89233218CNA000001.

- 
- [1] R. A. Hulse and J. H. Taylor, “Discovery of a pulsar in a binary system.” *Astrophysical Journal Letters* **195**, L51–L53 (1975).
  - [2] J. H. Taylor and J. M. Weisberg, “A new test of general relativity - Gravitational radiation and the binary pulsar PSR 1913+16,” *Astrophys. J.* **253**, 908–920 (1982).
  - [3] B. P. Abbott, R. Abbott, T. D. Abbott, F. Acernese, K. Ackley, C. Adams, T. Adams, P. Addesso, R. X. Adhikari, V. B. Adya, and et al., “GW170817: Observation of Gravitational Waves from a Binary Neutron Star Inspiral,” *Physical Review Letters* **119**, 161101 (2017), arXiv:1710.05832 [gr-qc].
  - [4] J. M. Lattimer and D. N. Schramm, “Black-Hole-Neutron-Star Collisions,” *Astrophysical Journal Letters* **192**, L145 (1974).
  - [5] Stephan Rosswog, “The multi-messenger picture of compact binary mergers,” *International Journal of Modern Physics D* **24**, 1530012-52 (2015), arXiv:1501.02081 [astro-ph.HE].
  - [6] Li-Xin Li and Bohdan Paczyński, “Transient Events from Neutron Star Mergers,” *Astrophysical Journal Letters* **507**, L59–L62 (1998).
  - [7] O. Korobkin, S. Rosswog, A. Arcones, and C. Winteler, “On the astrophysical robustness of the neutron star merger  $r$ -process,” *Monthly Notices of the Royal Astronomical Society* **426**, 1940–1949 (2012).
  - [8] Brian D. Metzger, “Kilonovae,” *Living Reviews in Relativity* **23** (2019), 10.1007/s41114-019-0024-0.
  - [9] John J. Cowan, Christopher Sneden, James E. Lawler, Ani Aprahamian, Michael Wiescher, Karlheinz Langanke, Gabriel Martínez-Pinedo, and Friedrich-Karl Thielemann, “Origin of the heaviest elements: The rapid neutron-capture process,” *Reviews of Modern Physics* **93**, 015002 (2021), arXiv:1901.01410 [astro-ph.HE].
  - [10] Jennifer Barnes, Y. L. Zhu, K. A. Lund, T. M. Sprouse, N. Vassh, G. C. McLaughlin, M. R. Mumpower, and R. Surman, “Kilonovae Across the Nuclear Physics Landscape: The Impact of Nuclear Physics Uncertainties on  $r$ -process-powered Emission,” *Astrophys. J.* **918**, 44 (2021), arXiv:2010.11182 [astro-ph.HE].
  - [11] Y. L. Zhu, K. A. Lund, J. Barnes, T. M. Sprouse, N. Vassh, G. C. McLaughlin, M. R. Mumpower, and

- R. Surman, “Modeling Kilonova Light Curves: Dependence on Nuclear Inputs,” *Astrophys. J.* **906**, 94 (2021).
- [12] Ryan T Wollaeger, Oleg Korobkin, Christopher J Fontes, Stephan K Rosswog, Wesley P Even, Christopher L Fryer, Jesper Sollerman, Aimee L Hungerford, Daniel R van Rossum, and Allan B Wollaber, “Impact of ejecta morphology and composition on the electromagnetic signatures of neutron star mergers,” *Monthly Notices of the Royal Astronomical Society* **478**, 3298–3334 (2018), <https://academic.oup.com/mnras/article-pdf/478/3/3298/25067894/sty1018.pdf>.
- [13] M. Ristic, E. Champion, R. O’Shaughnessy, R. Wollaeger, O. Korobkin, E. A. Chase, C. L. Fryer, A. L. Hungerford, and C. J. Fontes, “Interpolating detailed simulations of kilonovae: Adaptive learning and parameter inference applications,” *Physical Review Research* **4**, 013046 (2022), [arXiv:2105.07013](https://arxiv.org/abs/2105.07013) [astro-ph.HE].
- [14] C. Winteler, R. Käppeli, A. Perego, A. Arcones, N. Vasset, N. Nishimura, M. Liebendörfer, and F. K. Thielemann, “Magnetorotationally Driven Supernovae as the Origin of Early Galaxy r-process Elements?” *Astrophysical Journal Letters* **750**, L22 (2012).
- [15] Jennifer Barnes, Daniel Kasen, Meng-Ru Wu, and Gabriel Martínez-Pinedo, “Radioactivity and Thermalization in the Ejecta of Compact Object Mergers and Their Impact on Kilonova Light Curves,” *The Astrophysical Journal* **829**, 110 (2016).
- [16] C. J. Fontes, H. L. Zhang, J. Abdallah Jr., R. E. H. Clark, D. P. Kilcrease, J. Colgan, R. T. Cunningham, P. Hakel, N. H. Magee, and M. E. Sherrill, “The Los Alamos suite of relativistic atomic physics codes,” *Journal of Physics B Atomic Molecular Physics* **48**, 144014 (2015).
- [17] C. J. Fontes, C. L. Fryer, A. L. Hungerford, R. T. Wollaeger, and O. Korobkin, “A line-binned treatment of opacities for the spectra and light curves from neutron star mergers,” *Monthly Notices of the Royal Astronomical Society* **493**, 4143–4171 (2020).
- [18] Trevor Sprouse, Matthew Mumpower, Rebecca Surman, and Ani Aprahamian, “A generalized framework for nucleosynthesis calculations,” in *APS Division of Nuclear Physics Meeting Abstracts*, APS Meeting Abstracts, Vol. 2015 (2015) p. EA.097.
- [19] Oleg Korobkin, Ryan T. Wollaeger, Christopher L. Fryer, Aimee L. Hungerford, Stephan Rosswog, Christopher J. Fontes, Matthew R. Mumpower, Eve A. Chase, Wesley P. Even, Jonah Miller, G. Wendell Misch, and Jonas Lippuner, “Axisymmetric Radiative Transfer Models of Kilonovae,” *Astrophys. J.* **910**, 116 (2021).
- [20] A. Perego, S. Rosswog, R. M. Cabezón, O. Korobkin, R. Käppeli, A. Arcones, and M. Liebendörfer, “Neutrino-driven winds from neutron star merger remnants,” *Monthly Notices of the Royal Astronomical Society* **443**, 3134–3156 (2014), [arXiv:1405.6730](https://arxiv.org/abs/1405.6730) [astro-ph.HE].
- [21] S Rosswog, U Feindt, O Korobkin, M-R Wu, J Sollerman, A Goobar, and G Martinez-Pinedo, “Detectability of compact binary merger macronovae,” *Classical and Quantum Gravity* **34**, 104001 (2017).
- [22] David Radice, Albino Perego, Kenta Hotokezaka, Sebastiano Bernuzzi, Steven A. Fromm, and Luke F. Roberts, “Viscous-dynamical Ejecta from Binary Neutron Star Mergers,” *Astrophysical Journal Letters* **869**, L35 (2018), [arXiv:1809.11163](https://arxiv.org/abs/1809.11163) [astro-ph.HE].
- [23] Rodrigo Fernández, Alexander Tchekhovskoy, Eliot Quataert, Francois Foucart, and Daniel Kasen, “Long-term GRMHD simulations of neutron star merger accretion discs: implications for electromagnetic counterparts,” *Monthly Notices of the Royal Astronomical Society* **482**, 3373–3393 (2019), [arXiv:1808.00461](https://arxiv.org/abs/1808.00461) [astro-ph.HE].
- [24] Jonah M. Miller, Benjamin R. Ryan, Joshua C. Dolence, Adam Burrows, Christopher J. Fontes, Christopher L. Fryer, Oleg Korobkin, Jonas Lippuner, Matthew R. Mumpower, and Ryan T. Wollaeger, “Full transport model of GW170817-like disk produces a blue kilonova,” *Phys. Rev. D* **100**, 023008 (2019).
- [25] Vsevolod Nedora, Sebastiano Bernuzzi, David Radice, Boris Daszuta, Andrea Endrizzi, Albino Perego, Aviral Prakash, Mohammadtaher Safarzadeh, Federico Schianchi, and Domenico Logoteta, “Numerical Relativity Simulations of the Neutron Star Merger GW170817: Long-term Remnant Evolutions, Winds, Remnant Disks, and Nucleosynthesis,” *Astrophys. J.* **906**, 98 (2021), [arXiv:2008.04333](https://arxiv.org/abs/2008.04333) [astro-ph.HE].
- [26] Claudio Arlandini, Franz Käppeler, Klaus Wisshak, Roberto Gallino, Maria Lugaro, Maurizio Busso, and Oscar Straniero, “Neutron Capture in Low-Mass Asymptotic Giant Branch Stars: Cross Sections and Abundance Signatures,” *Astrophys. J.* **525**, 886–900 (1999), [arXiv:astro-ph/9906266](https://arxiv.org/abs/astro-ph/9906266) [astro-ph].
- [27] C. Sneden, J. J. Cowan, and R. Gallino, “Neutron-capture elements in the early galaxy,” *Annual Reviews of Astronomy and Astrophysics* **46**, 241–288 (2008).
- [28] Abdu Abohalima and Anna Frebel, “JINAbase—A Database for Chemical Abundances of Metal-poor Stars,” *Astroph. J. S.* **238**, 36 (2018), [arXiv:1711.04410](https://arxiv.org/abs/1711.04410) [astro-ph.SR].
- [29] Christopher Sneden, John J. Cowan, James E. Lawler, Inese I. Ivans, Scott Burles, Timothy C. Beers, Francesca Primas, Vanessa Hill, James W. Truran, George M. Fuller, Bernd Pfeiffer, and Karl-Ludwig Kratz, “The Extremely Metal-poor, Neutron Capture-rich Star CS 22892-052: A Comprehensive Abundance Analysis,” *Astrophys. J.* **591**, 936–953 (2003), [arXiv:astro-ph/0303542](https://arxiv.org/abs/astro-ph/0303542) [astro-ph].
- [30] W. Hayek, U. Wiesendahl, N. Christlieb, K. Eriksson, A. J. Korn, P. S. Barklem, V. Hill, T. C. Beers, K. Farouqi, B. Pfeiffer, and K.-L. Kratz, “The Hamburg/ESO R-process enhanced star survey (HERES). IV. Detailed abundance analysis and age dating of the strongly r-process enhanced stars CS 29491-069 and HE 1219-0312,” *Astronomy and Astrophysics* **504**, 511–524 (2009), [arXiv:0910.0707](https://arxiv.org/abs/0910.0707) [astro-ph.SR].
- [31] V. Hill, B. Plez, R. Cayrel, T. C. Beers, B. Nordström, J. Andersen, M. Spite, F. Spite, B. Barbuy, P. Bonifacio, E. Depagne, P. François, and F. Primas, “First stars. I. The extreme r-element rich, iron-poor halo giant CS 31082-001. Implications for the r-process site(s) and radioactive cosmochronology,” *Astronomy and Astrophysics* **387**, 560–579 (2002), [astro-ph/0203462](https://arxiv.org/abs/astro-ph/0203462).
- [32] J. Westin, C. Sneden, B. Gustafsson, and J. J. Cowan, “The r-Process-enriched Low-Metallicity Giant HD 115444,” *Astrophys. J.* **530**, 783–799 (2000), [astro-ph/9910376](https://arxiv.org/abs/astro-ph/9910376).
- [33] I. I. Ivans, J. Simmerer, C. Sneden, J. E. Lawler, J. J. Cowan, R. Gallino, and S. Bisterzo, “Near-Ultraviolet Observations of HD 221170: New Insights into the Na-

- ture of r-Process-rich Stars,” *Astrophys. J.* **645**, 613–633 (2006), [astro-ph/0604180](#).
- [34] J. J. Cowan, C. Sneden, S. Burles, I. I. Ivans, T. C. Beers, J. W. Truran, J. E. Lawler, F. Primas, G. M. Fuller, B. Pfeiffer, and K.-L. Kratz, “The Chemical Composition and Age of the Metal-poor Halo Star BD +17deg3248,” *Astrophys. J.* **572**, 861–879 (2002), [astro-ph/0202429](#).
- [35] J. Heinzl, M. W. Coughlin, T. Dietrich, M. Bulla, S. Antier, N. Christensen, D. A. Coulter, R. J. Foley, L. Issa, and N. Khetan, “Comparing inclination-dependent analyses of kilonova transients,” *Monthly Notices of the Royal Astronomical Society* **502**, 3057–3065 (2021).
- [36] Michael W. Coughlin, Tim Dietrich, Zoheyr Doctor, Daniel Kasen, Scott Coughlin, Anders Jerkstrand, Giorgos Leloudas, Owen McBrien, Brian D. Metzger, Richard O’Shaughnessy, and Stephen J. Smartt, “Constraints on the neutron star equation of state from AT2017gfo using radiative transfer simulations,” *Monthly Notices of the Royal Astronomical Society* **480**, 3871–3878 (2018).
- [37] Michael W. Coughlin, Tim Dietrich, Ben Margalit, and Brian D. Metzger, “Multimessenger Bayesian parameter inference of a binary neutron star merger,” *Monthly Notices of the Royal Astronomical Society* **489**, L91–L96 (2019).
- [38] V. A. Villar, J. Guillochon, E. Berger, B. D. Metzger, P. S. Cowperthwaite, M. Nicholl, K. D. Alexander, P. K. Blanchard, R. Chornock, T. Eftekhari, W. Fong, R. Margutti, and P. K. G. Williams, “The Combined Ultraviolet, Optical, and Near-infrared Light Curves of the Kilonova Associated with the Binary Neutron Star Merger GW170817: Unified Data Set, Analytic Models, and Physical Implications,” *Astrophysical Journal Letters* **851**, L21 (2017).
- [39] S. J. Smartt, T. W. Chen, A. Jerkstrand, M. Coughlin, E. Kankare, S. A. Sim, M. Fraser, C. Inserra, K. Maguire, K. C. Chambers, *et al.*, “A kilonova as the electromagnetic counterpart to a gravitational-wave source,” *Nature (London)* **551**, 75–79 (2017).
- [40] Matteo Breschi, Albino Perego, Sebastiano Bernuzzi, Walter Del Pozzo, Vsevolod Nedora, David Radice, and Diego Vescovi, “At2017gfo: Bayesian inference and model selection of multicomponent kilonovae and constraints on the neutron star equation of state,” *Monthly Notices of the Royal Astronomical Society* **505**, 1661–1677 (2021).
- [41] Matt Nicholl, Ben Margalit, Patricia Schmidt, Graham P. Smith, Evan J. Ridley, and James Nuttall, “Tight multimessenger constraints on the neutron star equation of state from gw170817 and a forward model for kilonova light-curve synthesis,” *Monthly Notices of the Royal Astronomical Society* **505**, 3016–3032 (2021).
- [42] Kamilė Lukošūtė, Geert Raaijmakers, Zoheyr Doctor, Marcelle Soares-Santos, and Brian Nord, “KilonovaNet: Surrogate Models of Kilonova Spectra with Conditional Variational Autoencoders,” arXiv e-prints, arXiv:2204.00285 (2022), [arXiv:2204.00285 \[astro-ph.IM\]](#).
- [43] P. Möller, A. J. Sierk, T. Ichikawa, and H. Sagawa, “Nuclear ground-state masses and deformations: FRDM(2012),” *Atomic Data and Nuclear Data Tables* **109**, 1–204 (2016), [arXiv:1508.06294 \[nucl-th\]](#).
- [44] J. M. Pearson, N. Chamel, A. F. Fantina, and S. Goriely, “Symmetry energy: nuclear masses and neutron stars,” *European Physical Journal A* **50**, 43 (2014), [arXiv:1309.2783 \[nucl-th\]](#).
- [45] I. V. Panov, I. Yu. Korneev, T. Rauscher, G. Martínez-Pinedo, A. Kelić-Heil, N. T. Zinner, and F. K. Thielemann, “Neutron-induced astrophysical reaction rates for translead nuclei,” *Astronomy and Astrophysics* **513**, A61 (2010), [arXiv:0911.2181 \[astro-ph.SR\]](#).
- [46] Mouza Almualla, Yuhong Ning, Mattia Bulla, Tim Dietrich, Michael W. Coughlin, and Nidhal Guesoum, “Using Neural Networks to Perform Rapid High-Dimensional Kilonova Parameter Inference,” arXiv e-prints, arXiv:2112.15470 (2021), [arXiv:2112.15470 \[astro-ph.HE\]](#).
- [47] Kyohei Kawaguchi, Masaru Shibata, and Masaomi Tanaka, “Diversity of Kilonova Light Curves,” *Astrophys. J.* **889**, 171 (2020).
- [48] David Radice, Filippo Galeazzi, Jonas Lippuner, Luke F. Roberts, Christian D. Ott, and Luciano Rezzolla, “Dynamical mass ejection from binary neutron star mergers,” *Monthly Notices of the Royal Astronomical Society* **460**, 3255–3271 (2016), [arXiv:1601.02426 \[astro-ph.HE\]](#).
- [49] Tim Dietrich, Sebastiano Bernuzzi, Maximiliano Ujevic, and Wolfgang Tichy, “Gravitational waves and mass ejecta from binary neutron star mergers: Effect of the stars’ rotation,” *Phys. Rev. D* **95**, 044045 (2017).
- [50] Masaru Shibata and Kenta Hotokezaka, “Merger and Mass Ejection of Neutron Star Binaries,” *Annual Review of Nuclear and Particle Science* **69**, 41–64 (2019), [arXiv:1908.02350 \[astro-ph.HE\]](#).
- [51] E. Troja, H. van Eerten, B. Zhang, G. Ryan, L. Piro, R. Ricci, B. O’Connor, M. H. Wieringa, S. B. Cenko, and T. Sakamoto, “A thousand days after the merger: Continued X-ray emission from GW170817,” *Monthly Notices of the Royal Astronomical Society* **498**, 5643–5651 (2020).
- [52] Khalil Farouqi, Friedrich-Karl Thielemann, Stephan Rosswog, and Karl-Ludwig Kratz, “Correlations of r-Process Elements in Very Metal-Poor Stars as Clues to their Nucleosynthesis Sites,” arXiv e-prints, arXiv:2107.03486 (2021), [arXiv:2107.03486 \[astro-ph.SR\]](#).
- [53] Sho Fujibayashi, Kenta Kiuchi, Shinya Wanajo, Koutarou Kyutoku, Yuichiro Sekiguchi, and Masaru Shibata, “Comprehensive study on the mass ejection and nucleosynthesis in the binary neutron star mergers leaving short-lived massive neutron stars,” arXiv e-prints, arXiv:2205.05557 (2022), [arXiv:2205.05557 \[astro-ph.HE\]](#).
- [54] Nicole Vassh, Gail C. McLaughlin, Matthew R. Mumpower, and Rebecca Surman, “The need for a local nuclear physics feature in the neutron-rich rare-earths to explain solar r-process abundances,” arXiv e-prints, arXiv:2202.09437 (2022), [arXiv:2202.09437 \[nucl-th\]](#).
- [55] I. Kullmann, S. Goriely, O. Just, R. Ardevol-Pulpillo, A. Bauswein, and H. T. Janka, “Dynamical ejecta of neutron star mergers with nucleonic weak processes I: nucleosynthesis,” *Monthly Notices of the Royal Astronomical Society* **510**, 2804–2819 (2022), [arXiv:2109.02509 \[astro-ph.HE\]](#).